Title

Thermal therapy of pancreatic tumours using endoluminal ultrasound: Parametric and patient-specific modelling

Journal

International Journal of Hyperthermia, 32(2)

ISSN

0265-6736

Authors

Adams, Matthew S
Scott, Serena J
Salgaonkar, Vasant A
et al.

Publication Date

2016-02-17

DOI

10.3109/02656736.2015.1119892

Peer reviewed

HHS Public Access

Author manuscript

Int J Hyperthermia. Author manuscript; available in PMC 2016 June 30.

Published in final edited form as:

Int J Hyperthermia. 2016 March ; 32(2): 97–111. doi:10.3109/02656736.2015.1119892.

Thermal therapy of pancreatic tumors using endoluminal ultrasound: parametric and patient-specific modeling

Matthew S. Adams[a,b,*], **Serena J. Scott**[a], **Vasant A. Salgaonkar**[a], **Graham Sommer**[c], and **Chris J. Diederich**[a,b]

[a]Thermal Therapy Research Group, University of California San Francisco, 2340 Sutter Street, S341, San Francisco, CA 94115

[b]University of California, Berkeley – University of California, San Francisco Graduate Program in Bioengineering, California

[c]Stanford Medical Center, 300 Pasteur Drive, Stanford, CA 94305

Abstract

Purpose—To investigate endoluminal ultrasound applicator configurations for volumetric thermal ablation and hyperthermia of pancreatic tumors using 3D acoustic and biothermal finite element models.

Materials and Methods—Parametric studies compared endoluminal heating performance for varying applicator transducer configurations (planar, curvilinear-focused, or radial-diverging), frequencies (1–5 MHz), and anatomical conditions. Patient-specific pancreatic head and body tumor models were used to evaluate feasibility of generating hyperthermia and thermal ablation using an applicator positioned in the duodenal or stomach lumen. Temperature and thermal dose were calculated to define ablation (>240 $EM_{43°C}$) and moderate hyperthermia (40–45 °C) boundaries, and to assess sparing of sensitive tissues. Proportional-integral control was incorporated to regulate maximum temperature to 70–80 °C for ablation and 45 °C for hyperthermia in target regions.

Results—Parametric studies indicated that 1–3 MHz planar transducers are most suitable for volumetric ablation, producing 5–8 cm^3 lesion volumes for a stationary 5 minute sonication. Curvilinear-focused geometries produce more localized ablation to 20–45 mm depth from the GI tract and enhance thermal sparing (T_{max}<42 °C) of the luminal wall. Patient anatomy simulations show feasibility in ablating 60.1–92.9% of head/body tumor volumes (4.3–37.2 cm^3) with dose <15 $EM_{43°C}$ in the luminal wall for 18–48 min treatment durations, using 1–3 applicator placements in GI lumen. For hyperthermia, planar and radial-diverging transducers could maintain up to 8 cm^3 and 15 cm^3 of tissue, respectively, between 40–45 °C for a single applicator placement.

*Contact Phone Number: (415) 476-8639, matt.adams@ucsf.edu.

7. **Declaration of interest:**

The work was supported by National Institutes of Health grant P01CA159992. This research was conducted with Government support under and awarded by DOD, Air Force Office of Scientific Research, National Defense Science and Engineering Graduate (NDSEG) Fellowship, 32 CFR 168a. The authors alone are responsible for the content and writing of the paper.

Conclusions—Modeling studies indicate the feasibility of endoluminal ultrasound for volumetric thermal ablation or hyperthermia treatment of pancreatic tumor tissue.

Keywords

Ultrasound; thermal therapy; pancreatic cancer; catheter-based ultrasound; thermal ablation; hyperthermia

2. Introduction

Pancreatic cancer causes the fourth highest number of cancer-related mortalities in the United States, and the current 5-year survival rate is 4% [1]. At clinical presentation, over 80% of patients are diagnosed with locally advanced or metastatic disease, which precludes curative treatment in the form of surgical resection [1]. The current standard clinical treatment for these patients involves gemcitabine-based chemotherapy with or without adjuvant radiation therapy, but these therapies have been shown to result in only modest survival and palliative benefit [2]. To relieve pain-related symptoms, which affects over 90% of advanced-staged patients, oral analgesics are typically administered; however, these require around-the-clock dosing for suitable palliation and have debilitating side effects, such as constipation [3,4]. Other current palliative techniques, such as alcohol ablation of the celiac plexus, have limited efficacy in some patients and may cause severe complications [4].

Thermal ablation has been applied for treatment of many malignancies, including cancers of the liver, lung, prostate, uterus, bone, and others [5]. It has also been demonstrated to provide palliative relief in patients with advanced pancreatic cancer through tumor debulking and neurolysis/denervation mechanisms, even in cases where only partial tumor volume ablation is achieved [6–9]. Ablation of locally advanced and metastatic pancreatic cancer can also potentially produce a survival advantage, as highlighted by recent efforts integrating high-intensity focused ultrasound (HIFU) ablation with chemotherapy [10]. Many ablative modalities, including radiofrequency ablation (RFA), cryoablation, microwave ablation, HIFU, photodynamic therapy, and electroporation are currently being developed or clinically investigated for treatment of pancreatic cancer [6]. With the exception of HIFU, all of these methods rely on invasive percutaneous or interstitial operation, which can be difficult to safely perform in the pancreas due to the close proximity of sensitive bowel tissues and major blood vessels, leading to many treatment-related complications [11]. As a result, better RFA treatment safety has been achieved by applying it in a laparotomy setting, which is highly invasive [11,12]. While HIFU is much less invasive than these other techniques, its application through the abdomen can be challenging and is precluded in many patients due to respiratory motion and obstructions in the acoustic pathway to the pancreas, caused by intervening organs, bowel, and gas within the GI tract [7,8].

In addition to thermal ablation, there is also potential clinical benefit in developing hyperthermia treatments for advanced pancreatic cancer. Pancreatic tumors are often characterized by hypovascularity, hypoxia, and desmoplastic stroma, which have been hypothesized to minimize the effectiveness of standard chemotherapy and radiation

treatments [13]. By transiently increasing the perfusion and oxygenation of treated tissues, hyperthermia has been shown to be an effective adjuvant therapy for both chemotherapy and radiation treatments in many cancer models [14–16]. Clinical studies evaluating the efficacy of combining regional hyperthermia and gemcitabine with or without cisplatin for patients with advanced pancreatic cancer have begun in both Europe and Japan [17,18]. Hyperthermia may also enhance the delivery of encapsulated drugs into desmoplastic pancreatic tumors through increasing local perfusion and, in the case of thermally sensitive drug-containing liposomes, directly triggering the release of the drug at the target site [19].

Endoluminal and intracavitary catheter-based ultrasound applicators can provide a minimally-invasive solution for delivery of thermal ablation or hyperthermia to tumors accessible from body lumens. Significant advantages of this ultrasound-based approach for thermal therapy include the high degree of control over the spatial distribution of energy as compared to other modalities, direct localization of the energy source and therapy adjacent to the target zone, as well as compatibility with diagnostic ultrasound or MR guidance techniques for possible real-time treatment monitoring and feedback control [20,21]. Specific applicator configurations for placement in the upper gastrointestinal (GI) tract have been applied clinically for endoluminal ablation of esophageal and biliary tumors [22,23]. An endoscope with a miniature spherically-focused transducer at the tip has also been developed and experimentally validated to create ablation lesions in porcine pancreas and liver under endoscopic ultrasound guidance [24,25].

Simulation studies incorporating parametric analysis and patient specific anatomical models have been applied for device design and performance evaluations of endoluminal and interstitial ultrasound technologies for thermal therapy (e.g. [26–33]). The objectives of this study are to investigate the feasibility and to characterize the performance of delivering volumetric thermal therapy to target regions within the pancreas using an endoluminal ultrasound applicator positioned within the GI tract. 3D acoustic and biothermal finite element models were developed to calculate power deposition patterns and resulting temperature and thermal dose distributions for both ablation and hyperthermia treatment paradigms. Full 3D multi-component models were used to perform parametric studies across applicator design parameters and anatomical variations to determine favorable designs and establish ranges of expected performance. Comprehensive patient-specific models, based on segmentation of CT images of pancreatic tumors and surrounding anatomy, were developed to serve as generalized anatomy models that bracket a range of representative geometries and potential target volumes. Using specific device configurations, as informed by the parametric studies, both thermal ablation and hyperthermia treatments were independently simulated in these models to evaluate delivery strategies and capabilities for achieving volumetric coverage of pancreatic tumor tissue while minimizing exposure to surrounding/intervening normal tissues.

3. Materials and Methods

3.1 Endoluminal Ultrasound Applicator

As shown in Figure 1, the endoluminal applicator would be inserted orally through the esophagus, and, akin to an endoscope, positioned in the stomach or duodenal lumen adjacent

to the tumor-bearing region of the pancreas. Acoustic energy would be directed through the GI luminal wall into the tumor by an ultrasound transducer array on the distal tip of the applicator. A balloon covering the transducers, containing circulating cooled water, would provide coupling of the acoustic energy into the adjacent tissue and cool the wall tissue to protect it from thermal injury.

The dimensions of the applicator and transducer assembly were conservatively chosen to be within a 15 mm diameter limit, following general constraints of the gastrointestinal anatomy on dimensions of endoscopic devices [34]. As illustrated in Figure 2, four separate transducer configurations were considered for this study: planar, tubular section, curvilinear along the azimuthal axis of the applicator (lightly focused), and curvilinear along the elevation axis (strongly focused). The dimensions of the planar and curvilinear transducers were modeled as 10 mm width × 20 mm length, and the tubular transducer was modeled with a 20 mm length, 80° active acoustic sector angle, and 6 mm radius of curvature. These geometries were chosen both due to their practical implementation and to examine diffuse vs. focal acoustic distributions. The distal tip of the applicator transducer assembly was modeled as a 12 mm diameter × 50 mm length cylinder with a single central transducer and the cooling balloon boundary situated 6.5 mm from the transducer surface, based off existing devices developed by our group.

3.2 Theory

3D acoustic and bioheat transfer models were implemented to calculate the acoustic intensity patterns and resulting transient temperature and thermal dose profiles produced by ultrasound applicators in an endoluminal anatomical setting. The preliminary modeling framework for endoluminal ablation of pancreatic tumors was developed by Prakash et. al., and expanded upon herein [35]. Temperature distributions were simulated using an implicit finite element method (FEM) solver (COMSOL Multiphysics 4.3, COMSOL, Inc.) and the Pennes bioheat transfer equation (Eq. 1) [36]:

$$\rho C\frac{dT}{dt}=\nabla[k\cdot\nabla T]-\omega_b C_b[T-T_b]+Q_{ac} \quad (1)$$

where ρ (kg m^{-3}) is tissue density, C (J kg^{-1} °C^{-1}) is the specific heat of tissue, T (°C) is tissue temperature, k (W m^{-1} °C^{-1}) is thermal conductivity, ω_b (kg m^{-3} s^{-1}) is blood perfusion, C_b (J kg^{-1} °C^{-1}) is the specific heat of blood, and T_b (°C) is capillary blood temperature (37 °C). Q_{ac} (W m^{-3}) is the acoustic heat deposition in tissue, and is derived from the acoustic pressure field (Eq. 2):

$$Q_{ac}=\frac{\alpha p_0^2}{\rho C} \quad (2)$$

where α (Np m^{-1}) is the acoustic absorption coefficient and p_0 (Pa) is the acoustic pressure amplitude. The acoustic absorption coefficient was approximated as equal to the acoustic attenuation coefficient μ (Np m^{-1}) for each tissue, as all scattered energy was assumed to be

absorbed locally. The acoustic pressure field was calculated for all considered transducer configurations using the Rayleigh-Sommerfeld diffraction integral, through a MATLAB (MathWorks, Inc.) implementation of the rectangular radiator approximation (Eq. 3) [37]:

$$p_0 = \frac{j\rho c \Delta w \Delta h}{\lambda} \sum_{n=1}^{N} \frac{u_n}{R} e^{(-\mu + jk)R} \operatorname{sinc}\left(\frac{kx_n \Delta w}{2R}\right) \operatorname{sinc}\left(\frac{ky_n \Delta h}{2R}\right) \quad (3)$$

where c (m s^{-1}) is the speed of sound, Δw and Δh (m) are the width and height of each rectangular sub-element, λ (m) is the wavelength, N is the total number of radiator sub-elements, R (m) is the distance from the radiator sub-element to the point in the tissue, k (m^{-1}) is the wavenumber, and x_n and y_n (m) are the difference in azimuthal and elevation coordinates between the tissue point and the radiator center. u_n (m s^{-1}) is the surface velocity for element n, and is calculated using the expression below (Eq. 4):

$$u_n = \sqrt{\frac{2I}{\rho c}} \quad (4)$$

where I is the transducer surface intensity (W m^{-2}), which is proportional to the electrical power applied to the transducer by the acoustic efficiency.

Temperature distributions were calculated using a direct implicit stationary solver (PARDISO) in COMSOL. Dirichlet boundary conditions constrained the outer boundaries of the tissue to 37°C, and a convective heat flux boundary condition was imposed at the balloon-tissue interface, with a heat transfer coefficient of h = 500 (W m^{-2} °C^{-1}) [38]. The range of temperatures for the cooling water flow was 7–25 °C, based on practical ranges typically used for ablation and hyperthermia devices. 7–10 °C cooling temperature was used for the ablation simulations to more efficiently reduce heating of the luminal wall. 20–25 °C water-cooling was applied in the hyperthermia simulations, with inherently lower applied power levels and resulting temperature and thermal dose, to avoid over-cooling and to extend therapeutic temperatures to tissue regions close to the luminal wall. Heterogenous tissue properties and perfusion values for stomach wall, duodenal wall, pancreas, tumor, and surrounding soft tissues were incorporated and are shown in Table I [39–44]. The material properties of pancreatic tumor tissue were assumed to be the same as pancreatic tissue, except for the attenuation coefficient where values equal to and slightly (1.25 times) higher than normal pancreatic tissue were included. This estimated higher value was used to account for the higher collagen content and fibrotic nature of the pancreatic tumor stroma, as collagen density has been shown to correlate with acoustic attenuation in other soft tissues [2,45,46]. While a range of attenuation values for pancreatic tissue was extracted from literature, and is specifically examined along with the corresponding tumor attenuation value in the parametric studies, all other modeling incorporated the highest values of these ranges, as shown in Table I, to give the most conservative estimates of achievable thermal lesion volumes and heating penetration. Proportional-integral (PI) feedback control of the applied power was integrated into the transient thermal solver, with the set-point evaluated between

70–80 °C to control the maximum temperature in the tumor. This controller was implemented to provide a standard point of comparison between simulations and to simulate a feasible feedback control scheme for treatment monitoring under either invasive thermometry or MR temperature imaging guidance [47]. Thermal dose distributions were calculated using the Sapareto-Dewey formulation (Eq. 5) [48]:

$$t_{43} = \sum_{t=0}^{t=final} R^{43-T} \Delta t \quad (5)$$

where t_{43} is the equivalent minutes at 43 °C ($EM_{43\,°C}$), R = 0.5 above 43 °C and 0.25 otherwise, and T is the average temperature at each point over a time interval Δt. The thermally destroyed or ablated tissue region was defined as the tissue in which the dose exceeded 240 $EM_{43\,°C}$, which has been shown to correspond to an approximate threshold for coagulative necrosis in many soft tissues [49–51]. In order to simulate the dynamic cessation of perfusion during ablation, a binary switch was implemented to reduce tissue perfusion from nominal to 0 kg m^{-3} s^{-1} during heating when tissue temperature exceeded 52 °C or thermal dose exceeded 300 $EM_{43\,°C}$ [52].

3.3 Parametric Studies

A simplified 3D model of a pancreatic head tumor, with surrounding normal pancreas and intervening tissue regions adjacent to the duodenum, was created (Figure 3) to provide the framework for parametric studies of general applicator design and performance. The applicator was positioned with the transducer off-set 6.5 mm from the duodenal wall, with water-cooling of the luminal wall surface adjacent to the applicator cooled by 10 °C or 25 °C water for ablation and hyperthermia treatments, respectively. The proximal edge of the pancreatic tumor tissue was 5 mm deep from the inner duodenal wall, and the overall dimensions of the tissue block were 50 × 50 × 73.5 mm. The duodenal luminal wall was modeled as distended with a 2 mm thickness [53]. Tissue thermal domains closer to the transducer were meshed at a finer resolution (equivalent to the acoustic wavelength) to appropriately capture the steep heating gradients near the applicator. The mesh size gradually increased to a maximum of 4 mm at the peripheral edges of the model. The acoustic calculations to obtain Q_{ac} were performed on a finer mesh (quarter-wavelength element length), which was then decimated to fit the thermal solver mesh. Convergence studies for both acoustic and bioheat transfer modeling were performed to ensure that the mesh element sizes were sufficiently small for accuracy and solution stability.

For parametric studies of ablation, the feedback controller was set to limit maximum tumor temperature to 80 °C. The following transducer design parameters were varied: the transducer configuration (planar, tubular section, lightly focused curvilinear, or strongly focused curvilinear), frequency (1–5 MHz), and the radius of curvature (ROC) for curvilinear geometries (15–100 mm). In order to capture the range of anatomical variation in adults, the duodenal wall thickness was varied between 1 and 5 mm. A range of values for the attenuation coefficient of pancreatic and tumor tissues, based off values reported in literature, was also incorporated. The range for pancreatic tissue was $4.37f^{1.2}$ Np/m –

$11.9f^{0.78}$ Np/m, and the tumor attenuation was varied between 1–1.25 times greater than the corresponding pancreatic value [39,54]. The effects of all of these parameters on the penetration depth of the thermal lesion, the total thermal lesion volume, and the maximum luminal wall temperature and thermal dose were evaluated. For each study, transient temperature solutions at a single applicator orientation were obtained with a variable time-stepping scheme for 5 minutes of total power application and heating time, followed by three minutes of cool-down with continued accrual of thermal dose and thermal spread of temperature contours. The PI controller proportional gain (K_p) and integral gain (K_i) parameters were adjusted for each case (K_p: 0.11–0.28 W °C^{-1}, K_i: 0.0012–0.005 W °C^{-1} s^{-1}) to achieve a 5 minute rise time to the maximum set-point temperature. This scheme was selected empirically to minimize power requirements and to set an appropriate time frame for image-guided control such as MRTI. It also resulted in minimal temperature overshoot and reduced thermal exposure of the luminal wall relative to shorter duration, high power schemes.

For parametric studies of hyperthermia, only the planar and tubular transducer configurations were considered, due to their larger volumetric coverage of heating. The frequency was varied between 1–4 MHz for both configurations, and the volumes and dimensions of the 40 °C and 43 °C contours were measured as endpoints. Simulations were designed to approach pseudo-steady state during 10 minute long transient solutions. The controller parameters, K_p and K_i, were chosen to elevate the max temperature to 45 °C within 2–3 minutes and sustain it for 7–8 additional minutes. These final isothermal contours approximate the steady-state hyperthermia distributions that could be maintained for desired treatment lengths.

3.4 Patient Anatomy Models

3D patient anatomy models were created based on axial CT imaging studies of patients with pancreatic cancer. Four geometries were incorporated, with details of each shown in Table II. These examples, while limited in representing the full scope of disease manifestation, were chosen to capture a range of distinct geometries, in terms of tumor size, location, and proximity to sensitive structures. Example 1 included a ~2 cm diameter pancreatic head tumor with boundaries immediately adjacent to the duodenum. Example 2 represents a ~2 cm diameter pancreatic head tumor located deeper (~5 mm from inner duodenal wall to closest proximity) in the pancreas and adjacent to the superior mesenteric artery (SMA), pancreatic duct, and bile duct. A strategy of preserving the bile duct during ablation treatment by using a simulated cooling balloon catheter was evaluated in this model. Example 3 represents a very advanced case, consisting of a large (~5 cm diameter) pancreatic head tumor close in proximity to the aorta, vena cava, portal vein, SMA, and superior mesenteric vein (SMV). While its size and proximity to vasculature may limit its candidacy for thermal therapy treatment, this model is incorporated in the analysis to investigate generalized heating performance and potential strategies that may be applicable in extreme cases. As such, multiple large position changes of the applicator along the duodenum were considered in this model to extend coverage of the tumor. Example 4 included a ~4 cm diameter pancreatic body tumor peripheral to the stomach, portal vein, SMV, splenic artery, splenic vein, hepatic artery, and the right gastroepiploic vein. In this

model sonication from the stomach lumen was simulated with a longer (10 × 30 mm) transducer geometry at two discrete applicator positions. For all cases, the applicator was rotated about the long (elevation) axis during therapy by discrete amounts in order to extend treatment coverage.

Mimics (Mimics Innovation Suite, Materialise) was used to segment the CT images and generate 3D surface meshes of nearby and relevant anatomical structures, including the tumor, pancreas, duodenum/stomach, luminal wall, ducts, and nearby significant vasculature in each model. Using 3-matic (Mimics Innovation Suite, Materialise), models of the applicator within a 2 cm diameter cooling balloon were positioned in either the duodenum or stomach lumen adjacent to the target volume, and the 3D object contours were converted into finite element meshes. Applicators were empirically positioned into a section of lumen close in proximity to the targeted region, such that large volumetric coverage of tissue could be achieved by rotation or minute translation of the applicator, and such that there were not sensitive structures (such as ducts, vessels) along the beam path. For models with multiple applicator positions, these placements were selected with the additional criteria that they should afford minimal overlap of thermal coverage. Interior luminal surfaces adjacent to the applicator were modeled as smooth, under the assumption that the cooling balloon provides distension of luminal folds with no trapped gas present at the interface. Convergence studies of mesh size were performed to ensure solution stability and accuracy, with a maximum mesh size of .75 mm in the region adjacent to the transducer surface extending 3–4 cm over the tumor volume, gradually transitioning to a maximum mesh size of 5–8 mm at the outer peripheries of the models. Each model consisted of 1.5–3 million elements, and Example 3 had three separate meshes which corresponded to the three distinct positions of the applicator.

Specific transducer configurations, empirically selected according to the model geometry and informed by the general performance characteristics revealed from the parametric studies, were chosen for ablation and hyperthermia simulations for each patient anatomy model. Each finite element mesh was imported into MATLAB for calculation of the acoustic intensity field using the rectangular radiator method, and all biothermal simulations were performed in COMSOL 4.3. Heterogeneous tissue properties, as shown in Table I, were incorporated. The attenuation coefficients of pancreatic and pancreatic tumor tissue were selected as the highest value in the aforementioned range ($11.9f^{0.78}$ and $1.25 \times 11.9f^{0.78}$, respectively). When visibly distended, ducts were modeled with the properties of static water. Localized cooling effects of major blood vessels were modeled using heat flux boundary conditions at the inner surface of the blood vessels, with an ambient blood temperature of 37 °C, and the heat transfer coefficient h value was calculated using the method detailed by Haemmerich et al., with vasculature parameters obtained from literature [55–60]. The duodenal and stomach walls were modeled as 2 mm and 3 mm thick, respectively [53,61,62]. Feedback control over the maximum tumor temperature was applied for the ablation simulations and transient temperature solutions were obtained. For hyperthermia studies, a single applicator position was considered. A constant input power to the transducer was applied to obtain temperature distributions at steady-state. Thermal treatment parameters, including cooling water temperature, maximum set-point temperature for the feedback controller, heating time lengths, and applicator orientations underwent

minor iteration for each case to limit thermal exposure to luminal and other sensitive tissues, and to extend volumetric coverage of tumor tissue, but were not rigorously optimized.

4. Results

4.1 Parametric Studies

The characteristic temperature and thermal dose contours produced by each transducer configuration for ablation treatment simulations are shown in Figure 4, for the frequency and curvatures specified in the caption. The effects of transducer configuration and frequency on ablation volume, penetration depth, and maximum luminal wall temperature/thermal dose are shown in Figure 5. The ablation volume for these five minute sonications ranged from 2.2–11.6 cm^3, and the penetration depth from the inner luminal wall into the targeted tumor tissue ranged from 18.6–43.4 mm depending on which configuration and frequency was used. Both frequency and transducer configuration had a significant effect on the sparing of the luminal wall, with the maximum temperature ranging from 37.3–44.5 °C at 1 MHz and 46.2–51.9 °C at 5 MHz across configurations. Maximum thermal dose exposure of the luminal wall exceeded 15 $EM_{43\ °C}$ for tubular transducers (at all frequencies), for planar and lightly curvilinear transducers operating at or above 4 MHz, and for strongly focused curvilinear transducers at 5 MHz.

For curvilinear transducer geometries, the effect of the degree of focusing on thermal lesions was examined by varying the radius of curvature (ROC) at a set frequency of 2 MHz, as shown by Figure 6. The influence of this parameter on the resulting lesion parameters was more pronounced with the strongly focused design. Increasing the radius curvature resulted in larger lesion volumes, ranging from 1.1–5.1 cm^3 as the ROC varied from 15–100 mm. A maximum penetration depth of 44.2 and 33.6 mm were obtained for the strongly focused and lightly focused transducers, respectively, at a 60 mm ROC. Sparing of the luminal wall was improved with lower ROCs down to approximately 20 mm, until the geometric focus of the transducer was within 10 mm of the luminal tissue.

As the luminal wall thickness increased from 1–5 mm, the maximal luminal wall temperature varied from 37.0–56.3 °C for planar, 37.0–54.8 °C for lightly focused curvilinear (30 mm ROC), 37.0–51.8 °C for strongly focused curvilinear (30 mm ROC), and 38.6–61.8 °C for tubular section transducers, all operating at 2 MHz. The relationship between luminal wall thickness and maximum wall temperature was approximately linear for all transducer configurations.

Sensitivity of the thermal lesion parameters to pancreatic and tumor attenuation coefficients varied with transducer configuration, as shown in Figure 7. For 2 MHz planar transducers, the lesion volume decreased 8.4–5.0 cm^3, the penetration depth decreased 50.5–34.5 mm, and the maximum luminal wall temperature increased 41.7–43 °C as pancreatic attenuation increased from $4.37f^{1.2}$ Np/m – $11.9f^{0.78}$ Np/m, with tumor attenuation 1.25x greater. When tumor attenuation was equal to pancreatic attenuation, the penetration depth and thermal lesion volume increased, by up to ~5 mm and 1 cm^3, respectively. The strongly focused transducer was insensitive to attenuation changes with regard to lesion volume, and the tubular section was relatively insensitive in terms of luminal heating. The penetration depths

of both configurations were less sensitive to attenuation compared to the planar and lightly focused transducers.

Parametric studies for hyperthermia treatments investigated the temperature distributions at steady-state, with maximum temperature set to 45 °C, and revealed similar trends as the ablation cases above. Tissue volumes elevated above 40 and 43 °C for the tubular section and planar transducers across 1–4 MHz frequencies are shown in Figure 8, in addition to the penetration depth of each temperature contour. The azimuthal extent of tubular section 40 and 43 °C contours were an average of 34.3 and 22.1 cm^3 across frequencies, while the same for the planar transducer were 14.2 and 7.4 cm^3, respectively. The contours' extents in the elevation direction were approximately equal (22.2 cm^3 and 15.1 cm^3 for tubular 40 and 43 °C contours vs. 21.8 cm^3 and 15.3 cm^3 for planar), and frequency independent. Maximum luminal temperatures for all tested configurations were below 39.5 °C, with maximum temperatures occurring with the 4 MHz tubular section configuration.

4.2 Patient Anatomy Models

Example 1 – Small Head Tumor—Ablation studies for this geometry (Figure 9) were simulated using an applicator placed in the duodenal lumen for two separate transducer configurations: a 2 MHz planar transducer and a 2 MHz lightly focused curvilinear transducer with an ROC of 25 mm. These were chosen due to the near proximity of the tumor boundary to the duodenal lumen and their capability to cover the majority of the tumor volume solely through rotation of the applicator. As shown in Table III, which details ablation treatment delivery parameters and results for all four cases, use of either configuration demonstrated ablation of over 90% of the tumor volume under twenty-five minutes without exceeding a duodenal wall thermal dose of 5 $EM_{43\,°C}$. More (5 vs. 3) discrete rotations of the applicator were necessary using the curvilinear transducer to extend tumor coverage. The curvilinear transducer resulted in a lower maximal thermal dose exposure of luminal tissue and the distal pancreatic duct.

Details of hyperthermia treatment simulations for all four geometries are shown in Table IV. A 1 MHz tubular transducer (80° active sector) was chosen for this geometry due to the relatively short depth of the tumor boundaries from the duodenum. With a constant applied surface intensity of 2.8 W/cm^2, 95% of the tumor volume could be elevated above 40 °C, as shown in Figure 9 (c). No rotation or translation of the applicator was necessary for full tumor coverage.

Example 2 – Small Head Tumor—The ablation study was simulated using an applicator placed in the duodenal lumen with a 2 MHz strongly focused curvilinear transducer (ROC of 32.5 mm) to more effectively target the deeper tumor depth and limit exposure to the adjacent sensitive tissues. Both rotation and minor translation (< 1 cm) of the applicator were necessary to increase tumor coverage. Over 80% of the tumor volume could be ablated in less than 20 min, with minimal thermal exposure to the SMA and pancreatic duct, as shown in Table III and Figure 10. Intraductal cooling of the bile duct using a simulated balloon catheter, with circulating coolant at 33 °C, was necessary to achieve adequate sparing of the bile duct, as shown in Figure 10 (b), for the simulated applicator

placements. Hyperthermia was performed with the applicator in a single position by rotating a 1.5 MHz planar transducer to cover the extent of the tumor, and could elevate 86.5% of the tumor volume above 40 °C at steady state, as shown in Figure 10 (c).

Example 3 – Large Head Tumor—Three discrete positions of the applicator along the length of the duodenum were used for the ablation study, as shown in Figure 11, with multiple rotations of the applicator at each position to increase tumor coverage. A planar 2 MHz transducer was chosen due to its large volumetric capabilities. Using this approach, about 60% of the 37 cm^3 volume could be ablated within 50 minutes of cumulative heating and cooling time. The maximal thermal doses applied to the adjacent vasculature, pancreatic duct, and duodenal wall were all less than 15 $EM_{43\,^\circ C}$. Within this same model, hyperthermia was simulated using a 1.5 MHz transducer at a single position shown in Figure 11 (c). With rotation of the applicator, 7.6 cm^3 (20.4%) of the tumor volume could be elevated above 40 °C at steady state.

Example 4 – Body Tumor—The applicator was positioned at two discrete locations in the stomach, and minutely translated and rotated at each to increase tumor coverage. For ablation, a 2 MHz planar transducer was chosen for volumetric capabilities, and generated ablation of 79.8% of the tumor volume in a 29 min total treatment time, as shown in Figure 12. Thermal damage to the 3 mm thick stomach wall was minimized (< 15 $EM_{43\,^\circ C}$) by using a lower cooling water temperature of 7 °C, and there was no substantial heating of the surrounding major blood vessels in the region (all < 1 $EM_{43\,^\circ C}$) or the pancreatic duct (< 5 $EM_{43\,^\circ C}$). For hyperthermia, a 1.5 MHz planar transducer was used at a single applicator position, and could elevate 66.6% of the tumor volume above 40 °C at steady state by rotating the applicator to cover the tumor extent, as shown in Figure 12 (c).

5. Discussion

This study has applied preliminary parametric and patient-specific acoustic and biothermal models to demonstrate the feasibility of generating ultrasound-based volumetric thermal ablation and hyperthermia within pancreatic tumors through the GI wall using an endoluminal delivery approach. Applicator transducer designs were investigated by evaluating four configurations (planer, lightly focused curvilinear, strongly focused curvilinear, and tubular section) across ranges of operating frequency and degree of focusing, with regard to heating capabilities and sparing of the luminal wall. Sweeps across transducer frequency for all configurations indicated that lower frequencies (1–3 MHz) were generally advantageous compared to higher frequencies (4–5 MHz), as they produced larger thermal lesion volumes and deeper penetration, while retaining the luminal wall at lower temperatures and thermal doses (Figure 5). In consideration of increased applied power requirements due to decreased absorption, cavitation thresholds within the applicator cooling fluid and tissue, and possibly excessive penetration of energy toward distal tissues and interfaces at frequencies at or below 1 MHz, a nominal low frequency of 2 MHz was selected for ablation simulations of the generalized patient anatomy models (Table III). With regards to heating characteristics of each transducer configuration, parametric studies revealed that the planar transducer has the most favorable general-performance profile: deep (~30–35 mm) penetration, high lesion volume capability (up to 6 cm^3 for a single position

and 5 minute application), and suitable sparing (T < 45 °C, dose < 10 $EM_{43\,°C}$) of the luminal wall at frequencies below 3 MHz (Figure 5). The strongly focused curvilinear transducer offers significantly superior sparing (3–4 °C lower max temperature, ~tenfold less thermal dose) of luminal tissue and the capability of tailoring the penetration and thermal lesion volume through *a priori* selection of the ROC (Figures 5, 6). These properties would make it appropriate as a more specialized design option, suitable for selective targeting of smaller target regions deeper from the GI tract or sonication through thicker (> 3 mm) luminal walls. Lightly curvilinear transducers represent an intermediate between the planar and strongly focused designs, allowing some control over heating depth and volumetric coverage (Figures 5, 6), but without a distinct significant advantage. Ablation studies across varying normal pancreatic and tumor tissue attenuation coefficients revealed that heating characteristics of focused transducers were less influenced by tissue attenuation as compared to the more diffuse configurations (Figure 7). Thus, in the absence of quantitative tissue property measurements, focused transducer designs could be advantageous due to their more predictable and consistent performance. Tubular sector transducers, in contrast, were demonstrably the least suitable for ablation due to shallow heat penetration and comparably higher thermal exposure (4–7 °C higher max temperature) of the luminal wall relative to other configurations (Figure 5). However, low-frequency tubular transducers could be appropriate for delivering hyperthermia to small target volumes within 3 cm of the luminal wall (Figure 9). Planar transducer devices would require rotation to cover equivalent azimuthal extent, but could be advantageous for generating hyperthermia within larger/deeper targets due to greater penetration and potential volumetric coverage. As an alternative to having an assortment of these fixed transducer configurations available for a procedure, it may be possible to incorporate a more complex phased array transducer capable of dynamically producing variations of these focused and diffuse beam patterns, thereby permitting more flexibility from a single device in treatment delivery [63–65].

One of the primary safety requisites for endoluminal ultrasound delivery of thermal ablation to pancreatic targets is precluding thermal damage to the stomach or duodenal wall. This concern is relatively minimal for hyperthermia delivery, due to the much lower temperature elevation requirements, as shown by the parametric studies. While specific thermal dose thresholds of thermal damage for human duodenal or stomach wall tissues have not been distinctly established, approximate damage thresholds can be inferred from experimental investigations in porcine GI tract (esophagus, small intestine, rectum) [66–68]. These studies indicate that significant acute and chronic damage, including degenerative necrosis of the tissue or thromboses of blood vessels, occur at thermal dose levels greater than 80–120 $EM_{43\,°C}$ and temperatures greater than 45–47 °C [67,68]. As such, the maximum luminal temperatures and doses obtained in the ablation simulations for the patient anatomy model studies (< 45 °C and < 15 $EM_{43\,°C}$) were considered to be within the safe limit to avoid significant thermal injury. As shown by the parametric studies, maximum luminal wall thermal exposures were strongly dependent on the luminal wall thickness. As such, sonicating through the stomach wall would likely have a higher risk of thermal injury as compared to through the duodenal wall, due to its greater thickness. However, there are many treatment parameters that could be adjusted to compensate for the increased risk of sonication through thicker GI luminal walls, including lowering the maximum set-point

temperature or decreasing the cooling water flow temperature, as shown in the body tumor model (Figure 12). Using more focused transducer configurations, tailoring the ROC, and/or using lower frequency transducers could also improve sparing of the luminal wall (Figures 5, 6). In practice, it could be beneficial to distend the stomach or duodenum lumen to stretch and thin the luminal wall. This would be particularly important in the presence of folds or rugae, which could cause an increase in effective wall thickness or harbor air bubbles that could impact acoustic transmission and increase localized heating [25]. Distension of the lumens may be achievable either through filling the stomach or small intestines with water, through endoscopic manipulation, or by incorporating large distensible balloons onto the applicator that would be inflated once the applicator was positioned [69].

Simulations of these applicators incorporating patient anatomy models of pancreatic tumors and surrounding tissues illustrated feasibility of safely generating conformal ablation or hyperthermia across a range of tumor positions, sizes, and applicator positioning. Positioning the applicator within the duodenum provided the most access to tumors in the head of the pancreas (Figures 9–11), whereas the body tumor was most accessible to an applicator placed in the stomach lumen (Figure 12). All models necessitated sequential rotation and/or repositioning of the applicator to extend coverage of tumor volumes, leading to slightly scalloped or irregular outer boundaries of the lesions, as typical for heating with discretely rotating planar and curvilinear devices [70]. Substantial portions (> 80% of total volume) of head tumors under 3 cm diameter could be targeted for ablative or hyperthermic temperature exposures in short (< 30 minutes) heating times without any major applicator repositions (Figures 9, 10). Furthermore, fewer manipulations were needed for applicators with a planar transducer as compared to lightly or strongly focused transducer configurations, due to its greater volumetric coverage (Figure 9 (b)). However, tailoring the ROC of focused transducers to the target anatomy provided more preferential heating of the tumor and enhanced sparing of normal tissues proximal/distal to the tumor, as compared to the non-focused geometry (Table III, Figure 9 (b)). Obtaining suitable volumetric ablation of large pancreatic tumors (> 4 cm diameter) places additional demands on applicator positioning and manipulation to access different portions of the tumor, as shown in Figure 11. These large target volumes and re-positional requirements could increase technical and time demands, and may be impractical for extended hyperthermia delivery, depending upon temperature range and time regimen required. In addition to size, the proximity of pancreatic tumors to sensitive anatomy, such as ducts, bowel, or significant vasculature, limits volumetric tumor coverage for ablation and imposes the need for highly accurate placement and manipulation of the applicator to ensure that energy is directed precisely towards target tissues. Integrating the applicator with an endoscope may provide sufficient control for positional accuracy [25]. Image-guidance techniques, incorporating MRI or ultrasound guidance, could also be employed to verify positioning, monitor treatments, and permit feedback control [25,71,72]. While the PI feedback control scheme employed herein permitted conformal lesion formation, more advanced schemes incorporating pilot/boundary-control points or model predictive control could further improve targeting and reduce undesirable thermal exposure [52,73]. Additional strategies to preserve sensitive tissues, such as internal cooling of major ducts using a cooling catheter, as shown in Figure 10 (b), may be considered. Further optimization of designs and delivery strategies can be

achieved with more extensive modeling inclusive of additional and broader ranges of patient anatomy cases.

In principle, this endoluminal ultrasound approach may offer significant advantages over existing techniques for delivering thermal therapy to the pancreas. It can provide an attractive alternative to percutaneous RF or microwave ablation by minimizing complication risk through much more selective and targeted heating, and would not require major open surgery for its application [6,11,12]. Compared to extracorporeal HIFU, endoluminal ultrasound could provide overall shorter ablation treatment times or enhanced hyperthermia coverage due to its local volumetric heating capability (Tables III, IV). It could also provide easier access to tumors near or invading the duodenum or bowels that are often acoustically inaccessible from extracorporeal sources [7–9]. Further, although not investigated herein, application of these devices from within the body also suggests that in terms of energy delivery, compensating for respiratory or other sources of motion may be less challenging as compared to extracorporeal HIFU due to tissue and applicator motion being constrained together through endoscopic fixation. However, integrating the endoluminal approach with image-guidance treatment monitoring and feedback, e.g. by using MR thermometry, could still require respiratory gating or other motion-compensatory techniques [71].

6. Conclusion

3D acoustic and biothermal models illustrate the feasibility of generating ultrasound-based thermal therapy within pancreatic tumors using an endoluminal applicator placed in the duodenal or stomach lumen. Four specific applicator transducer configurations, ranging from curvilinear-focused to planar or radial-diverging, were demonstrated to provide appreciable volumetric coverage for thermal ablation of pancreatic tumors or the delivery of moderate hyperthermia. Planar and curvilinear configurations could produce ablative temperatures and lethal thermal doses for tissue volumes of up to 8 cm^3 for a single applicator placement and 5 minute sonication length, and for larger tumors additional rotations or translations of the applicator could be used to extend coverage. For moderate hyperthermia delivery, non-focused transducer geometries could sustain up to 16 cm^3 of target tissue between a temperature range of 40–45 °C. Thermal simulations provide preliminary guidelines for appropriate frequency, transducer geometry, positioning, and treatment parameters to deliver conformal thermal therapy to pancreatic head or body target regions ranging from 20–45 mm deep from the GI wall while minimizing thermal exposures (dose < 15 $EM_{43°C}$) to the intervening stomach or duodenal tissues. Additional modeling in the form of parametric studies and patient anatomy models can be applied for further optimization of device designs and delivery approaches.

References

1. American Cancer Society. Cancer Facts & Figures, 2013. 2013.
2. Stathis A, Moore MJ. Advanced pancreatic carcinoma: current treatment and future challenges. Nat Rev Clin Oncol. 2010; 7(3):163–172. [PubMed: 20101258]
3. Brescia FJ. Palliative care in pancreatic cancer. Cancer Control. 2004; 11(1):39–45. [PubMed: 14749622]

4. Hameed M, Hameed H, Erdek M. Pain management in pancreatic cancer. Cancers. 2010; 3(1):43–60. [PubMed: 24212605]
5. Diederich CJ. Thermal ablation and high-temperature thermal therapy: overview of technology and clinical implementation. Int J Hyperthermia. 2005; 21(8):745–753. [PubMed: 16338857]
6. Keane MG, Bramis K, Pereira SP, Fusai GK. Systematic review of novel ablative methods in locally advanced pancreatic cancer. World J Gastroenterol. 2014; 20(9):2267. [PubMed: 24605026]
7. Zhou Y. High-intensity focused ultrasound treatment for advanced pancreatic cancer. Gastroenterol Res Pract. 2014; 2014:1.
8. Anzidei M, Marincola BC, Bezzi M, Brachetti G, Nudo F, Cortesi E, et al. Magnetic resonance-guided high-intensity focused ultrasound treatment of locally advanced pancreatic adenocarcinoma: preliminary experience for pain palliation and local tumor control. Invest Radiol. 2014 Dec; 49(12): 759–765. [PubMed: 24932986]
9. Wu F, Wang Z, Zhu H, Chen W, Zou J, Bai J, et al. Feasibility of US-guided high-intensity focused ultrasound treatment in patients with advanced pancreatic cancer: initial experience. Radiology. 2005; 236(3):1034–1040. [PubMed: 16055692]
10. Vidal-Jove J, Perich E, del Castillo MA. Ultrasound guided high intensity focused ultrasound for malignant tumors: the Spanish experience of survival advantage in stage III and IV pancreatic cancer. Ultrason Sonochem. 2015; 27:703–6. [PubMed: 26044461]
11. Pezzilli R, Ricci C, Serra C, Casadei R, Monari F, D'Ambra M, et al. The problems of radiofrequency ablation as an approach for advanced unresectable ductal pancreatic carcinoma. Cancers. 2010; 2(3):1419–1431. [PubMed: 24281165]
12. Girelli R, Frigerio I, Salvia R, Barbi E, Tinazzi Martini P, Bassi C. Feasibility and safety of radiofrequency ablation for locally advanced pancreatic cancer. Br J Surg. 2010; 97(2):220–225. [PubMed: 20069610]
13. Rasheed, ZA.; Matsui, W.; Maitra, A. Pathology of pancreatic stroma in PDAC. In: Grippo, PJ.; Munshi, HG., editors. Pancreatic Cancer and Tumor Microenvironment. Trivandrum (India): Transworld Research Network; 2012.
14. Diederich CJ, Hynynen K. Ultrasound technology for hyperthermia. Ultrasound Med Biol. 1999; 25(6):871–887. [PubMed: 10461714]
15. Issels RD. Hyperthermia adds to chemotherapy. Eur J Cancer. 2008; 44(17):2546–2554. [PubMed: 18789678]
16. Issels RD, Lindner LH, Verweij J, Wust P, Reichardt P, Schem B, et al. Neo-adjuvant chemotherapy alone or with regional hyperthermia for localised high-risk soft-tissue sarcoma: a randomised phase 3 multicentre study. Lancet Oncol. 2010; 11(6):561–570. [PubMed: 20434400]
17. Tschoep-Lechner KE, Milani V, Berger F, Dieterle N, Abdel-Rahman S, Salat C, et al. Gemcitabine and cisplatin combined with regional hyperthermia as second-line treatment in patients with gemcitabine-refractory advanced pancreatic cancer. Int J Hyperthermia. 2013; 29(1): 8–16. [PubMed: 23245336]
18. Ishikawa T, Kokura S, Sakamoto N, Ando T, Imamoto E, Hattori T, et al. Phase II trial of combined regional hyperthermia and gemcitabine for locally advanced or metastatic pancreatic cancer. Int J Hyperthermia. 2012; 28(7):597–604. [PubMed: 22838644]
19. Needham D, Dewhirst MW. The development and testing of a new temperature-sensitive drug delivery system for the treatment of solid tumors. Adv Drug Deliv Rev. 2001; 53(3):285–305. [PubMed: 11744173]
20. Salgaonkar VA, Diederich CJ. Catheter-based ultrasound technology for image-guided thermal therapy: Current technology and applications. Int J Hyperthermia. 2015; 31(2):203–215. [PubMed: 25799287]
21. Lafon C, Melodelima D, Salomir R, Chapelon JY. Interstitial devices for minimally invasive thermal ablation by high-intensity ultrasound. Int J Hyperthermia. 2007; 23(2):153–163. [PubMed: 17578339]
22. Melodelima D, Prat F, Fritsch J, Theillere Y, Cathignol D. Treatment of esophageal tumors using high intensity intraluminal ultrasound: first clinical results. J Transl Med. 2008; 6:28. [PubMed: 18533990]

23. Lafon C, Theillere Y, Prat F, Arefiev A, Chapelon J, Cathignol D. Development of an interstitial ultrasound applicator for endoscopic procedures: animal experimentation. Ultrasound Med Biol. 2000; 26(4):669–675. [PubMed: 10856631]
24. Hwang JH, Farr N, Morrison K, Wang Y, Khokhlova T, Ko B, et al. 876 Development of an EUS-guided high-intensity focused ultrasound endoscope. Gastrointest Endosc. 2011; 73(4):AB155.
25. Li T, Khokhlova T, Maloney E, Wang Y, D'Andrea S, Starr F, et al. Endoscopic high-intensity focused US: technical aspects and studies in an in vivo porcine model (with video). Gastrointest Endosc. 2015; 81(5):1243–1250. [PubMed: 25759124]
26. Prakash P, Salgaonkar VA, Diederich CJ. Modelling of endoluminal and interstitial ultrasound hyperthermia and thermal ablation: Applications for device design, feedback control and treatment planning. Int J Hyperthermia. 2013; 29(4):296–307. [PubMed: 23738697]
27. Chen X, Diederich CJ, Wootton JH, Pouliot J, Hsu I. Optimisation-based thermal treatment planning for catheter-based ultrasound hyperthermia. Int J Hyperthermia. 2010; 26(1):39–55. [PubMed: 20100052]
28. Scott SJ, Salgaonkar V, Prakash P, Burdette EC, Diederich CJ. Interstitial ultrasound ablation of vertebral and paraspinal tumours: Parametric and patient-specific simulations. Int J Hyperthermia. 2014; 30(4):228–244. [PubMed: 25017322]
29. Chopra R, Burtnyk M, Haider MA, Bronskill MJ. Method for MRI-guided conformal thermal therapy of prostate with planar transurethral ultrasound heating applicators. Phys Med Biol. 2005; 50(21):4957. [PubMed: 16237234]
30. Wootton JH, Prakash P, Hsu IJ, Diederich CJ. Implant strategies for endocervical and interstitial ultrasound hyperthermia adjunct to HDR brachytherapy for the treatment of cervical cancer. Phys Med Biol. 2011; 56(13):3967. [PubMed: 21666290]
31. Chopra R, Burtnyk M, N'djin WA, Bronskill M. MRI-controlled transurethral ultrasound therapy for localised prostate cancer. Int J Hyperthermia. 2010; 26(8):804–821. [PubMed: 21043572]
32. Burtnyk M, Chopra R, Bronskill MJ. Quantitative analysis of 3-D conformal MRI-guided transurethral ultrasound therapy of the prostate: Theoretical simulations. Int J Hyperthermia. 2009; 25(2):116–131. [PubMed: 19337912]
33. Burtnyk M, Chopra R, Bronskill M. Simulation study on the heating of the surrounding anatomy during transurethral ultrasound prostate therapy: A 3D theoretical analysis of patient safety. Med Phys. 2010; 37(6):2862–2875. [PubMed: 20632598]
34. Varadarajulu S, Banerjee S, Barth BA, Desilets DJ, Kaul V, Kethu SR, et al. GI endoscopes. Gastrointest Endosc. 2011; 74(1):1–6. e6. [PubMed: 21704803]
35. Prakash P, Salgaonkar VA, Scott SJ, Jones P, Hensley D, Holbrook A, et al. MR guided thermal therapy of pancreatic tumors with endoluminal, intraluminal and interstitial catheter-based ultrasound devices: Preliminary theoretical and experimental investigations. Proc SPIE. 2013 85840V-85840V-10.
36. Pennes HH. Analysis of tissue and arterial blood temperatures in the resting human forearm. J Appl Physiol. 1948 Aug; 1(2):93–122. [PubMed: 18887578]
37. Ocheltree KB, Frizzel L. Sound field calculation for rectangular sources. IEEE Trans Ultrason Ferroelectr Freq Control. 1989; 36(2):242–248. [PubMed: 18284974]
38. Wootton JH, Hsu IJ, Diederich CJ. Endocervical ultrasound applicator for integrated hyperthermia and HDR brachytherapy in the treatment of locally advanced cervical carcinoma. Med Phys. 2011; 38(2):598–611. [PubMed: 21452697]
39. Duck, Francis A. Physical properties of tissues: a comprehensive reference book. London: Academic press; 2013.
40. Hasgall P, Neufeld E, Gosselin M. IT'IS Database for thermal and electromagnetic parameters of biological tissues. 2013 Version 2.4, July 30th, 2013.
41. Kersting S, Konopke R, Kersting F, Volk A, Distler M, Bergert H, et al. Quantitative perfusion analysis of transabdominal contrast-enhanced ultrasonography of pancreatic masses and carcinomas. Gastroenterology. 2009; 137(6):1903–1911. [PubMed: 19715694]
42. Caldwell CB, Ricotta JJ. Changes in visceral blood flow with elevated intraabdominal pressure. J Surg Res. 1987; 43(1):14–20. [PubMed: 3599981]

43. Delrue L, Blanckaert P, Mertens D, Van Meerbeeck S, Ceelen W, Duyck P. Tissue perfusion in pathologies of the pancreas: assessment using 128-slice computed tomography. Abdom Imaging. 2012; 37(4):595–601. [PubMed: 21811851]
44. Kandel S, Kloeters C, Meyer H, Hein P, Hilbig A, Rogalla P. Whole-organ perfusion of the pancreas using dynamic volume CT in patients with primary pancreas carcinoma: acquisition technique, post-processing and initial results. Eur Radiol. 2009; 19(11):2641–2646. [PubMed: 19471941]
45. O'Donnell M, Mimbs J, Miller J. The relationship between collagen and ultrasonic attenuation in myocardial tissue. J Acoust Soc Am. 1979; 65(2):512–517. [PubMed: 489819]
46. Imamura T, Iguchi H, Manabe T, Ohshio G, Yoshimura T, Wang Z, et al. Quantitative analysis of collagen and collagen subtypes I, III, and V in human pancreatic cancer, tumor-associated chronic pancreatitis, and alcoholic chronic pancreatitis. Pancreas. 1995; 11(4):357–364. [PubMed: 8532652]
47. Smith N, Merrilees N, Hynynen K, Dahleh M. Control system for an MRI compatible intracavitary ultrasound array for thermal treatment of prostate disease. Int J Hyperthermia. 2001; 17(3):271–282. [PubMed: 11347731]
48. Sapareto SA, Dewey WC. Thermal dose determination in cancer therapy. Int J Radiat Oncol Biol Phys. 1984; 10(6):787–800. [PubMed: 6547421]
49. McDannold N, Hynynen K, Wolf D, Wolf G, Jolesz F. MRI evaluation of thermal ablation of tumors with focused ultrasound. J Magn Reson Imaging. 1998; 8(1):91–100. [PubMed: 9500266]
50. Dewey WC. Arrhenius relationships from the molecule and cell to the clinic. Int J Hyperthermia. 2009; 25(1):3–20. [PubMed: 19219695]
51. Yarmolenko PS, Moon EJ, Landon C, Manzoor A, Hochman DW, Viglianti BL, et al. Thresholds for thermal damage to normal tissues: an update. Int J Hyperthermia. 2011; 27(4):320–343. [PubMed: 21591897]
52. Prakash P, Diederich CJ. Considerations for theoretical modelling of thermal ablation with catheter-based ultrasonic sources: Implications for treatment planning, monitoring and control. Int J Hyperthermia. 2012; 28(1):69–86. [PubMed: 22235787]
53. Masselli G, Picarelli A, Di Tola M, Libanori V, Donato G, Polettini E, et al. Celiac Disease: Evaluation with Dynamic Contrast-enhanced MR Imaging. Radiology. 2010; 256(3):783–790. [PubMed: 20663971]
54. Jones JP, Behrens M. In vivo measurement of frequency dependent attenuation in normal liver, pancreas, and spleen. Ultrason Imaging. 1981; 3(2):205–206.
55. Haemmerich D, Wright A, Mahvi D, Lee F Jr, Webster J. Hepatic bipolar radiofrequency ablation creates coagulation zones close to blood vessels: a finite element study. Med Biol Eng Comput. 2003; 41(3):317–323. [PubMed: 12803297]
56. Arienti V, Califano C, Brusco G, Boriani L, Biagi F, Giulia Sama M, et al. Doppler ultrasonographic evaluation of splanchnic blood flow in coeliac disease. Gut. 1996 Sep; 39(3): 369–373. [PubMed: 8949639]
57. Perišić MD, Ćulafić D, Kerkez M. Specificity of splenic blood flow in liver cirrhosis. Rom J Intern Med. 2005; 43(1–2):141–151. [PubMed: 16739874]
58. Hübner GH, Steudel N, Kleber G, Behrmann C, Lotterer E, Fleig WE. Hepatic arterial blood flow velocities: assessment by transcutaneous and intravascular Doppler sonography. J Hepatol. 2000; 32(6):893–899. [PubMed: 10898309]
59. Chato J. Heat transfer to blood vessels. J Biomech Eng. 1980; 102(2):110–118. [PubMed: 7412233]
60. Gabe IT, Gault JH, Ross J Jr, Mason DT, Mills CJ, Schillingford JP, et al. Measurement of instantaneous blood flow velocity and pressure in conscious man with a catheter-tip velocity probe. Circulation. 1969 Nov; 40(5):603–614. [PubMed: 5377202]
61. Nylund K, Hausken T, Ødegaard S, Eide G, Gilja O. Gastrointestinal wall thickness measured with transabdominal ultrasonography and its relationship to demographic factors in healthy subjects. Ultraschall Med. 2012; 33(7):E225. [PubMed: 22504939]
62. Zuber-Jerger I, Muller A, Kullmann F, Gelbmann CM, Endlicher E, Muller-Ladner U, et al. Gastrointestinal manifestation of systemic sclerosis--thickening of the upper gastrointestinal wall

detected by endoscopic ultrasound is a valid sign. Rheumatology. 2010 Feb; 49(2):368–372. [PubMed: 20008473]

63. Melodelima D, Salomir R, Mougenot C, Moonen C, Cathignol D. 64-element intraluminal ultrasound cylindrical phased array for transesophageal thermal ablation under fast MR temperature mapping: an ex vivo study. Med Phys. 2006; 33(8):2926–2934. [PubMed: 16964871]
64. Pichardo S, Hynynen K. New design for an endoesophageal sector-based array for the treatment of atrial fibrillation: a parametric simulation study. IEEE Trans Ultrason Ferroelectr Freq Control. 2009; 56(3):600–612. [PubMed: 19411218]
65. Werner J, Park E, Lee H, Francischelli D, Smith NB. Feasibility of in vivo transesophageal cardiac ablation using a phased ultrasound array. Ultrasound Med Biol. 2010; 36(5):752–760. [PubMed: 20347517]
66. Date RS, Biggins J, Paterson I, Denton J, McMahon RF, Siriwardena AK. Development and validation of an experimental model for the assessment of radiofrequency ablation of pancreatic parenchyma. Pancreas. 2005; 30(3):266–271. [PubMed: 15782106]
67. Dewhirst M, Viglianti B, Lora-Michiels M, Hanson M, Hoopes P. Basic principles of thermal dosimetry and thermal thresholds for tissue damage from hyperthermia. Int J Hyperthermia. 2003; 19(3):267–294. [PubMed: 12745972]
68. Li D, Zhou S, Qiu S, Qiao S. Thermodamage, thermosensitivity and thermotolerance of normal swine oesophagus. Int J Hyperthermia. 1987; 3(2):143–151. [PubMed: 3598250]
69. Bhutani, MS.; Deutsch, JC. EUS Pathology with Digital Anatomy Correlation: A Text and Atlas. Shelton, CT: PMPH-USA; 2009.
70. Ross AB, Diederich CJ, Nau WH, Rieke V, Butts RK, Sommer G, et al. Curvilinear transurethral ultrasound applicator for selective prostate thermal therapy. Med Phys. 2005; 32(6):1555–1565. [PubMed: 16013714]
71. Rieke V, Butts Pauly K. MR thermometry. J Magn Reson Imaging. 2008; 27(2):376–390. [PubMed: 18219673]
72. Ebbini ES, Ter Haar G. Ultrasound-guided therapeutic focused ultrasound: Current status and future directions. Int J Hyperthermia. 2015; 31(2):77–89. [PubMed: 25614047]
73. Arora D, Cooley D, Perry T, Skliar M, Roemer RB. Direct thermal dose control of constrained focused ultrasound treatments: phantom and in vivo evaluation. Phys Med Biol. 2005; 50(8):1919. [PubMed: 15815104]

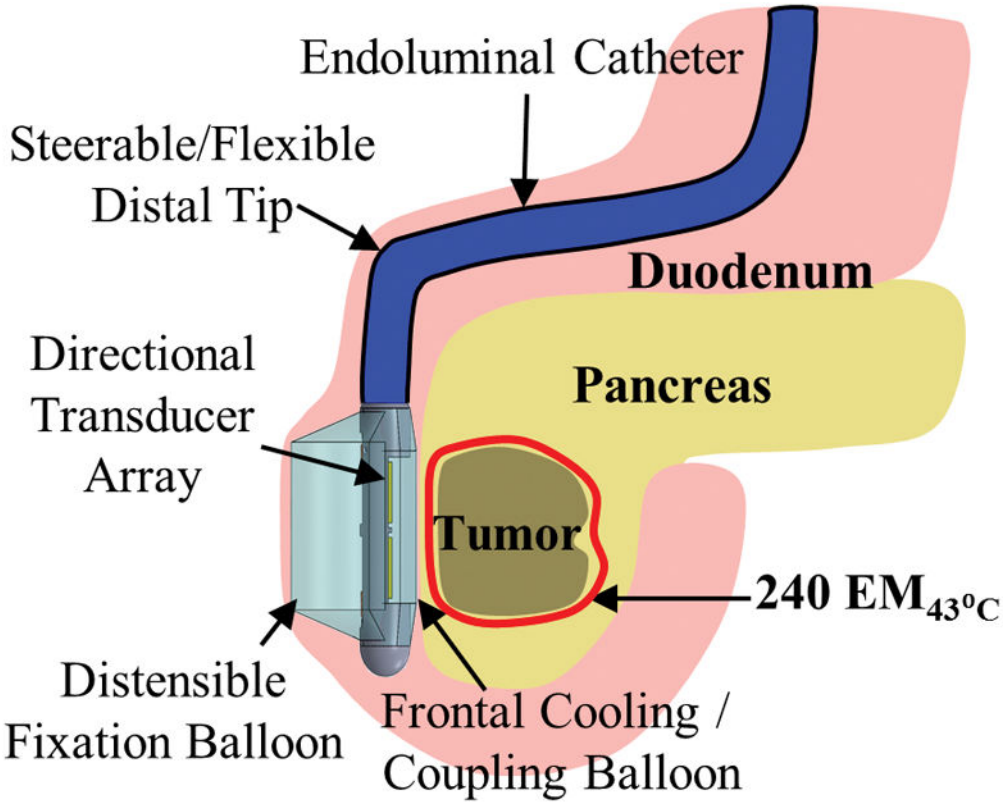

Figure 1.

Schema and concepts of an endoluminal ultrasound applicator positioned in the GI tract for thermal therapy of pancreatic tumors. The applicator is illustrated as positioned in the duodenum for sonication of tumors in the head of the pancreas, following placement and insertion strategies common in endoscopy. Transducer arrays are configured for focused or diffuse patterns to provide a high degree of spatial control and volumetric heating.

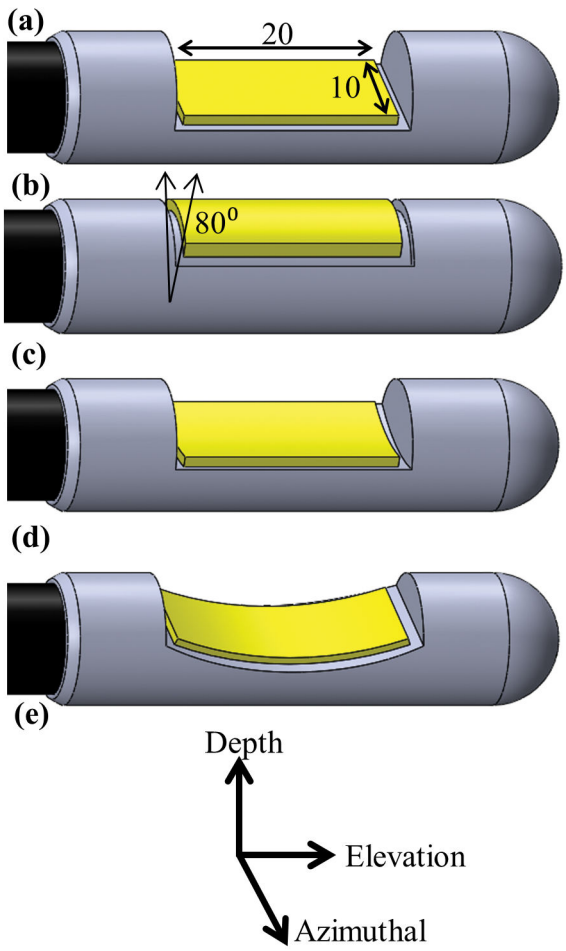

Figure 2.

Considered transducer (yellow) configurations: (a) planar, (b) tubular section, (c) lightly focused curvilinear along the azimuthal direction, and (d) strongly focused curvilinear along the elevation direction, with respect to the (e) transducer coordinate system. The planar and curvilinear transducers are 20 × 10 mm along the elevation and azimuthal directions, and the tubular section is an 80° sector with a 6 mm radius of curvature and a 20 mm length.

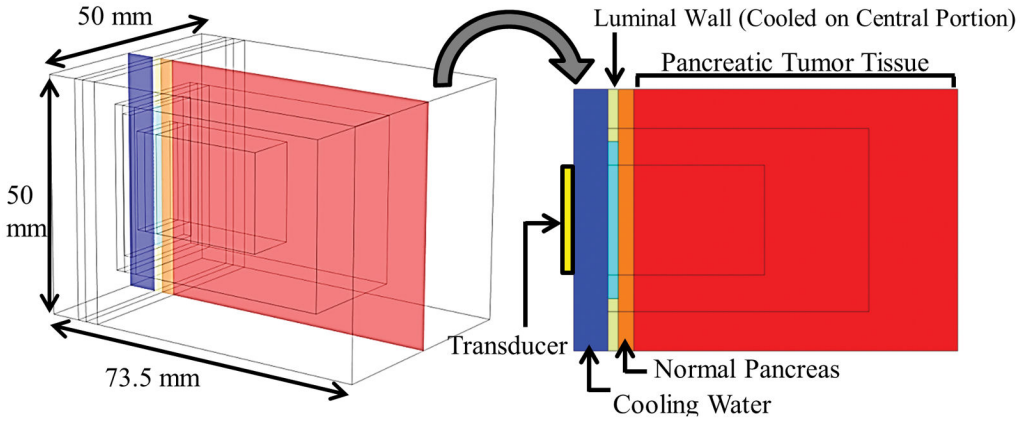

Figure 3.

3D generalized pancreatic tumor model employed for parametric studies of endoluminal ultrasound thermal therapy.

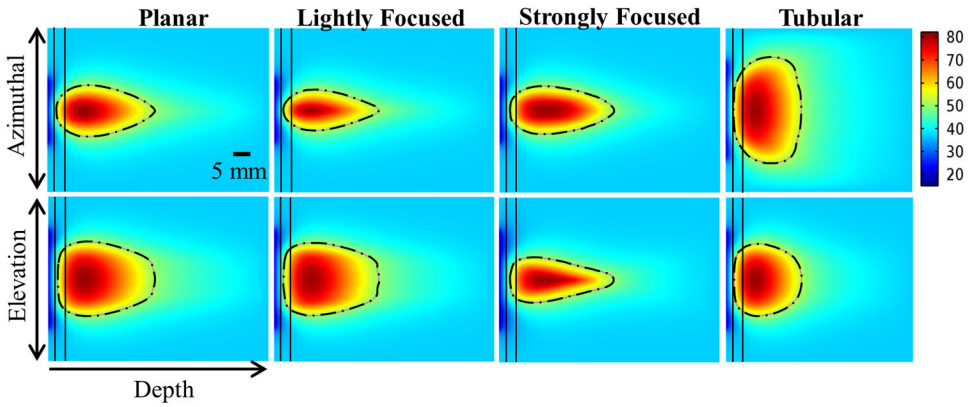

Figure 4.

Cross-sectional temperature distributions and 240 $EM_{43°C}$ contours (black dashes) for ablation studies in the generalized tumor model for 10 × 20 mm planar, lightly focused, strongly focused, and 80° tubular transducer configurations operating at 2 MHz, after 5 minutes of active sonication.

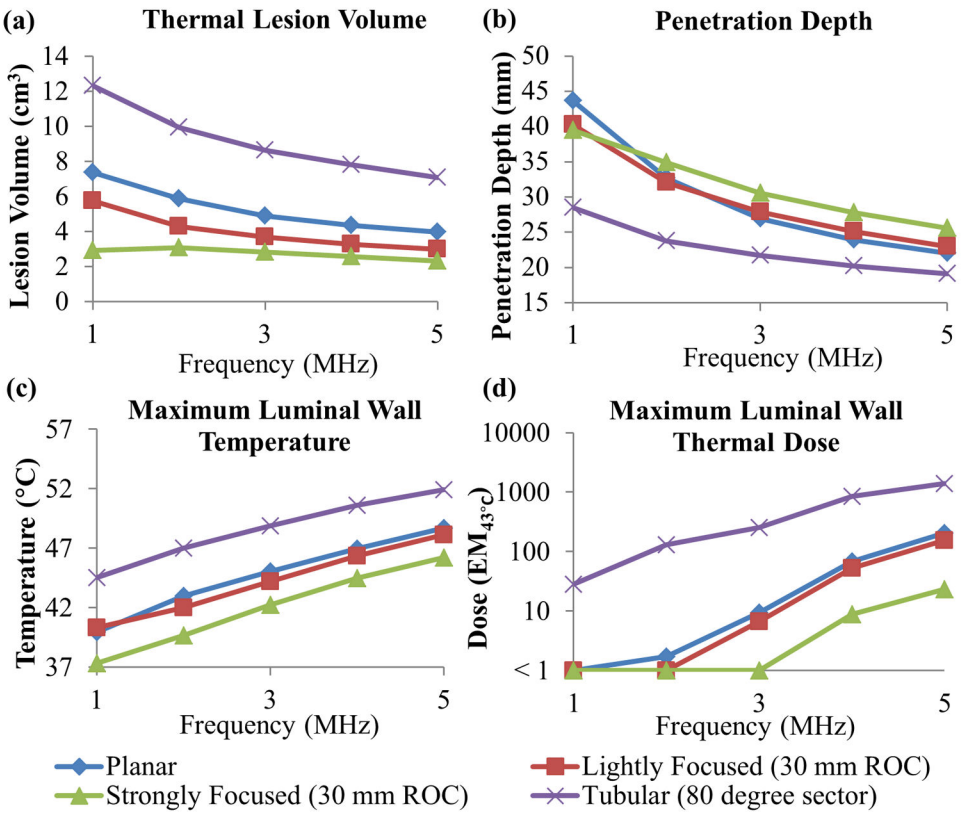

Figure 5.

Effects of transducer configuration and operating frequency on (a) tumor ablation volume (thermal dose > 240 $EM_{43\,°C}$), (b) penetration depth (measured from inner luminal wall) of thermal lesion, and maximum (c) temperature and (d) thermal dose of luminal wall tissue, after a single 5 minute sonication with a temperature set-point of 80 °C and 3 minutes of post-sonication cooling.

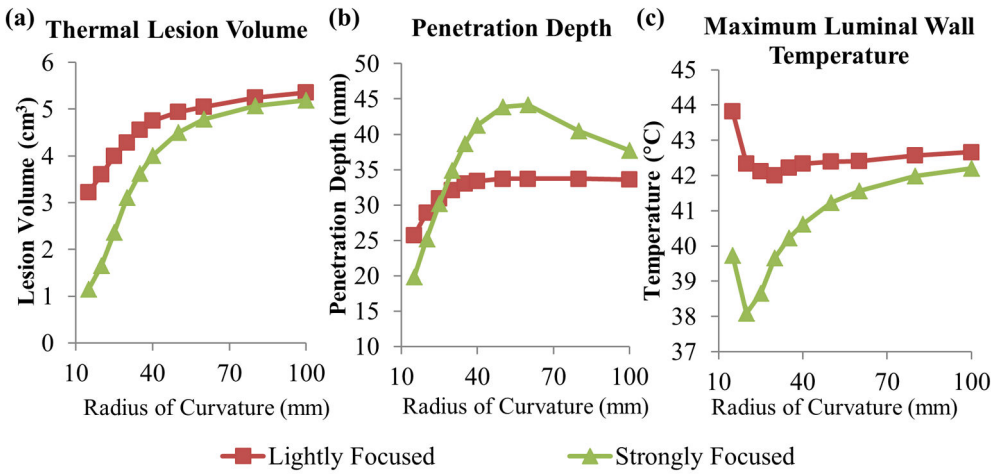

Figure 6.

Effects of radius of curvature for 2 MHz curvilinear transducers on (a) tumor ablation volume (dose > 240 $EM_{43\,°C}$), (b) penetration depth (measured from inner luminal wall) of thermal lesion, and (c) maximum temperature of luminal wall tissue, after a single 5 minute sonication with a temperature set-point of 80 °C and 3 minute post-sonication cooling.

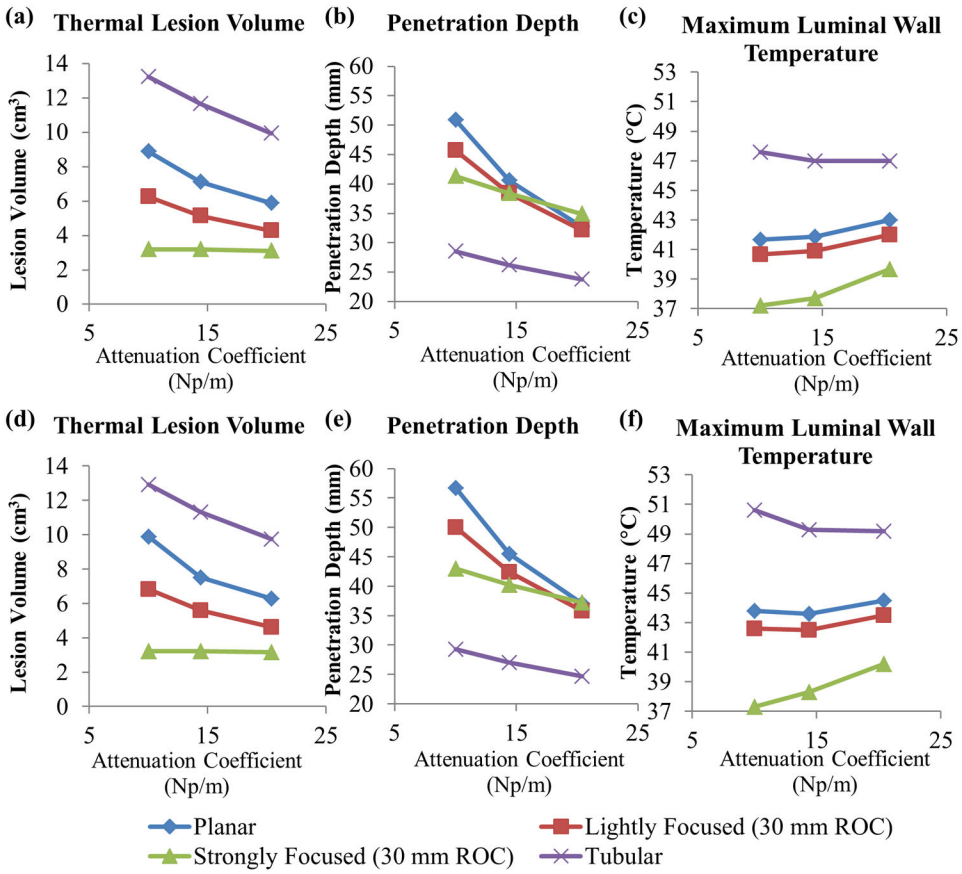

Figure 7.

Effects of pancreatic tissue attenuation coefficient on (a, d) tumor ablation volume (dose > 240 $EM_{43\ °C}$), (b, e) penetration depth (measured from inner luminal wall) of thermal lesion, and (c, f) maximum temperature of luminal wall tissue, after a single 5 minute sonication at 2 MHz operating frequency, with a maximum temperature set-point of 80 °C and 3 minute post-sonication cooling period. The tumor attenuation coefficient is 1.25x the corresponding pancreatic tissue attenuation in (a)–(c), and equivalent to the pancreatic tissue attenuation in (d)–(f).

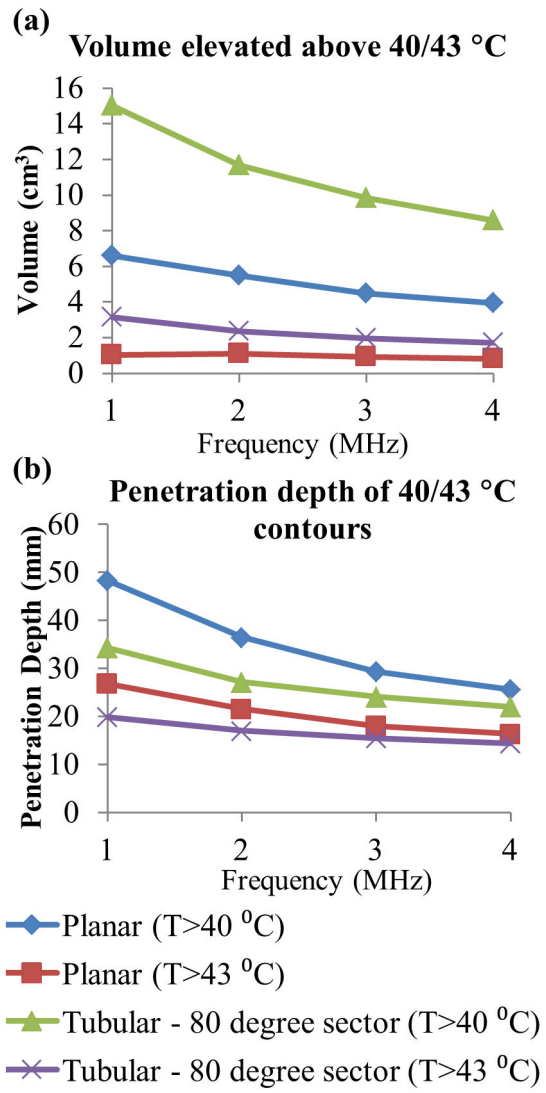

Figure 8.

Effects of transducer configuration and operating frequency on (a) tumor volume elevated above 40 and 43 °C, and penetration depth (measured from inner luminal wall) of 40 and 43 °C temperature contours, at steady-state with a maximum temperature set-point of 45 °C for generation of moderate hyperthermia.

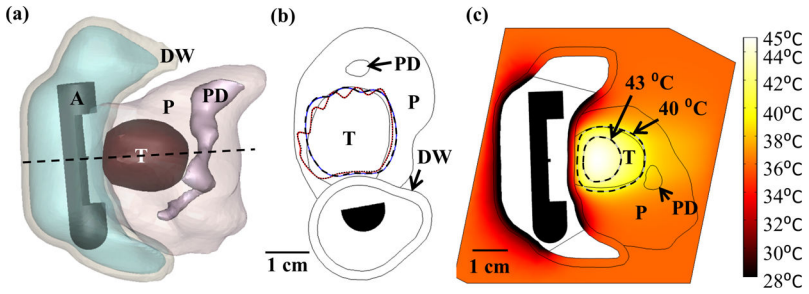

Figure 9.

(a) 3D model of the Example 1 anatomy, consisting of a small pancreatic head tumor directly adjacent to the duodenal lumen and positioned applicator. (b) 240 $EM_{43\ °C}$ contours for ablation simulations using a 2 MHz planar (blue with dashes) and 2 MHz lightly focused curvilinear transducer with a 25 mm ROC (red with dots) across the central transverse slice through the applicator. (c) Temperature distributions and 40 and 43 °C contours (grey with dashes) are given for a hyperthermia simulation using a 1 MHz tubular section transducer. A: applicator, T: tumor, P: pancreas, DW: duodenal wall, PD: pancreatic duct.

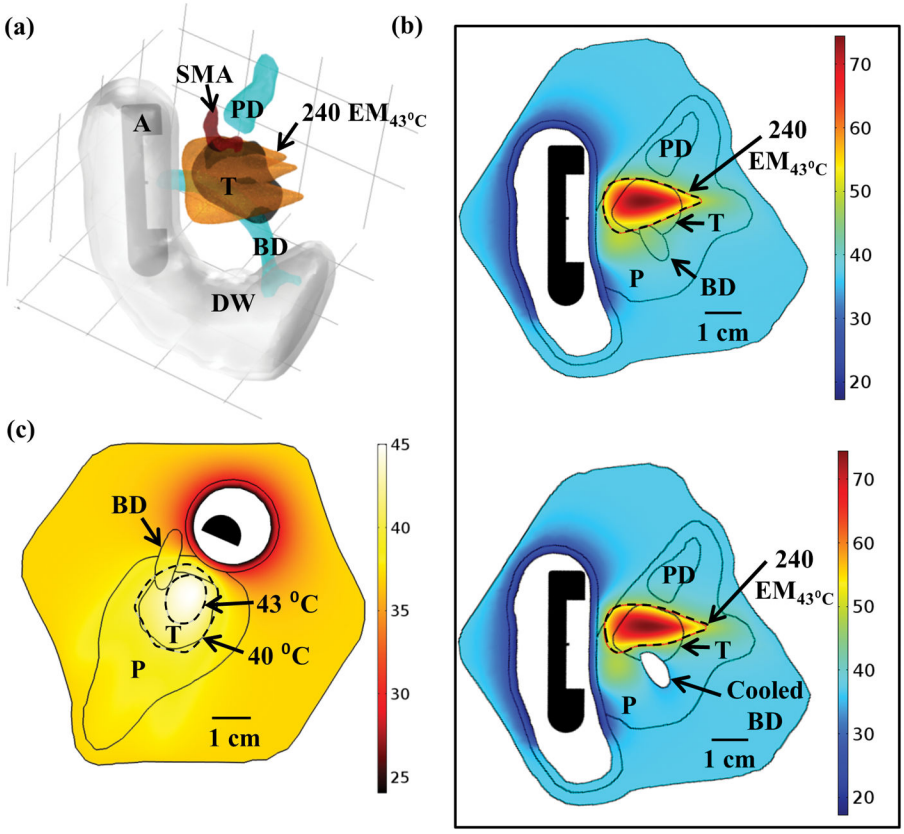

Figure 10.

(a) Ablated lesion volume (dose > 240 $EM_{43\,°C}$) overlaid with the Example 2 model anatomy, consisting of a small head tumor surrounded by the SMA, PD, and BD, using a 2 MHz strongly focused curvilinear transducer. (b) Maximum temperatures and 240 $EM_{43\,°C}$ contours across a sagittal plane for two ablation simulations: without (top) and with (bottom) simulated cooling of the bile duct, all other treatment parameters being identical. Sparing of the bile duct (BD) could be achieved by perfusing it with cooling water during the duration of the ablation treatment. (c) Temperature distributions and 40 and 43 °C contours (grey with dashes) for hyperthermia produced by rotating a 1.5 MHz planar applicator. A: applicator, T: tumor, P: pancreas, DW: duodenal wall, PD: pancreatic duct, BD: bile duct, SMA: superior mesenteric artery.

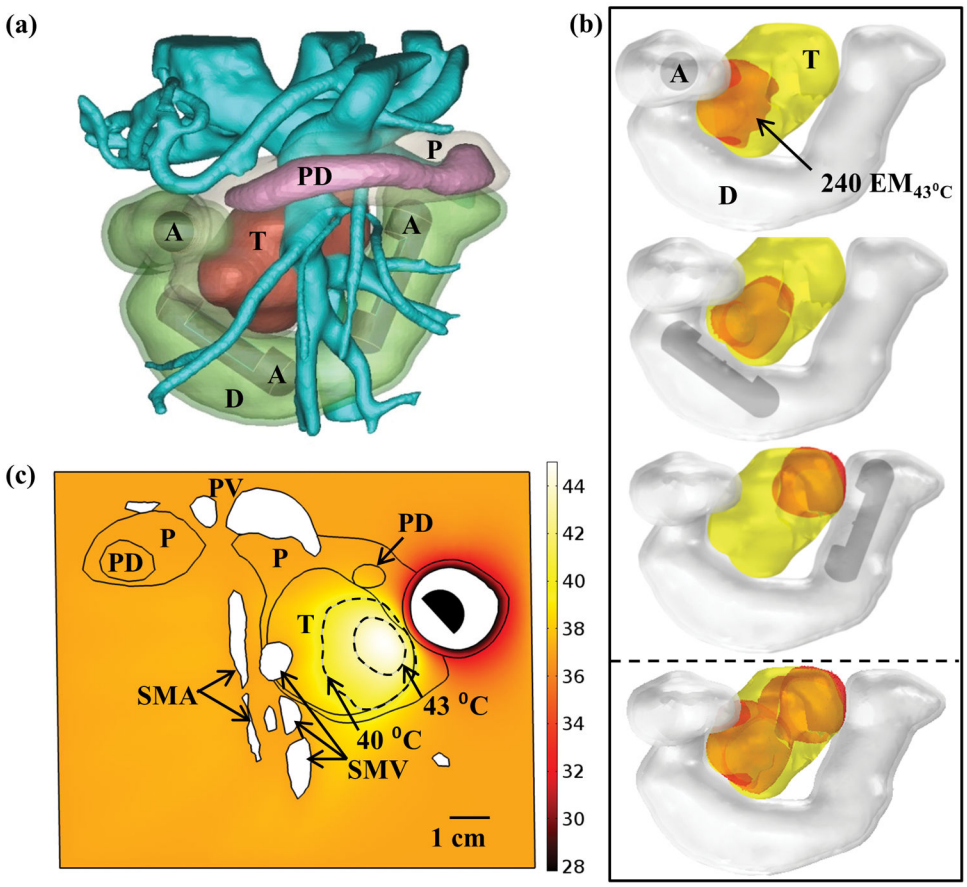

Figure 11.

(a) 3D model of the Example 3 large pancreatic head tumor and surrounding anatomy, illustrating proximity of tumor to significant vasculature. (b) Ablated lesions (orange) were produced in the tumor by translating an applicator with a 2 MHz planar transducer to three individual positions along the length of the duodenum, with the cumulative thermal lesion shown at the bottom. (c) Temperature distribution and 40 and 43 °C contours (grey with dashes) across an axial plane for hyperthermia simulation using a 1.5 MHz planar transducer, rotated at a single position in the duodenum. A: applicator, T: tumor, P: pancreas, D: duodenum, PD: pancreatic duct, PV: portal vein, SMV: superior mesenteric vein, SMA: superior mesenteric artery.

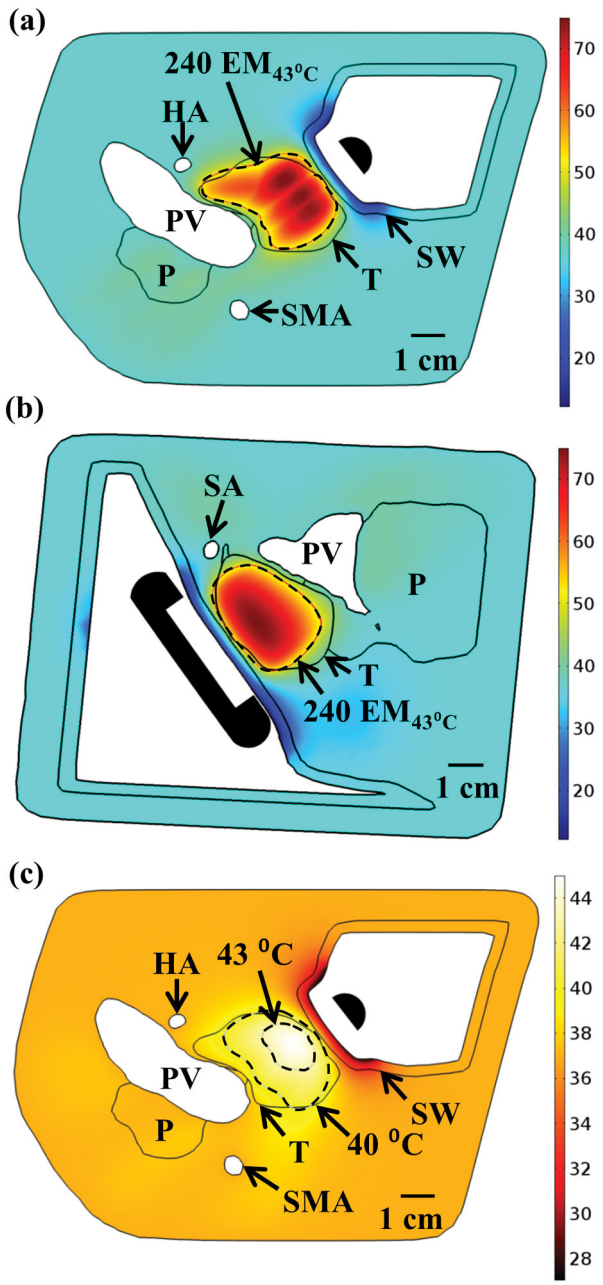

Figure 12.

Maximum temperature distributions and 240 $EM_{43\ ^{\circ}C}$ contours (dashed) across (a) axial and (b) sagittal planes after ablation treatment for the Example 4 body tumor model, as treated with an applicator positioned in the stomach lumen with a 30×10 mm 2 MHz planar transducer. (c) Temperature distribution and 40 and 43 °C contours (grey) across an axial slice for hyperthermia by rotating a 1.5 MHz planar applicator. T: tumor, SW: stomach wall, P: pancreas, PV: portal vein, SMA: superior mesenteric artery, HA: hepatic artery, SA: splenic artery.

Table I

Material properties used in acoustic and biothermal modeling. *f*: frequency (MHz).

Tissue	Density (kg/m^3)	Attenuation (Np/m)	Thermal Conductivity (W/m/°C)	Specific Heat (J/kg/°C)	Perfusion Rate (kg/m^3/s)
Pancreas	1045 (1)	$11.9f^{0.78}$ (1)	0.51 (2)	3164 (2)	10 (1)
Pancreatic Tumor	1045	$1.25 \times 11.9f^{0.78}$	0.51	3164	4.5 (3, 5, 6)
Stomach Wall	1045 (2)	$5f^{*}$	0.53 (2)	3698 (2)	6.75 (1, 4)
Duodenal Wall	1045 (2)	$5f^{*}$	0.53 (2)	3698 (2)	16.67 (1)
Soft Tissue	1045 (1)	$6.4f$ (1)	0.49 (2)	3421 (2)	3 (1)
Blood	1050 (2)	$1.6f^{1.21}$ (1)	0.52 (2)	3617 (2)	

*Estimated from lab attenuation measurements in porcine stomach tissue (data not shown).

Table II

General anatomical characteristics of patient anatomy models of pancreatic tumors. PD: pancreatic duct, BD: bile duct, SMA: superior mesenteric artery, VC: vena cava, PV: portal vein, SMV: superior mesenteric vein, SV: splenic vein, RGV: right gastroepiplioc vein, HA: hepatic artery, SA: splenic artery.

Case	Tumor location	Applicator placement	Tumor vol. (cm^3)	Tumor dim. (mm)	Nearest distance of tumor to inner luminal wall (mm)	Distances from tumor to sensitive anatomical structures (mm)	
1	Head	Duodenum	4.3	21 × 19 × 18	2	PD – 1.5	
2	Head	Duodenum	4.3	17 × 22 × 24	5	PD – 3 SMA – 0	SD – 0
3	Head	Duodenum	37.2	50 × 44 × 25	2.5	PD – 0 Aorta – 2 SMV – 0	VC – 3 PV – 6 SMA – 1.5
4	Body	Stomach	17.5	45 × 25 × 25	4.5	PD – 0 SMV – 1 RGV – 1 SA – 1	PV – 0.5 SV – 1 HA – 4

Table III

Parameters and outcomes for patient anatomy ablation simulations. DW: duodenal wall, PD: pancreatic duct, BD: bile duct, BV: blood vessels, SW: stomach wall.

Case	Transducer Configuration	Freq. (MHz)	Max set-point temp. (°C)	Cooling water temp. (°C)	Total time (min)	% Tumor ablated	Max Temperature/Dose on Sensitive Anatomy
1	Planar	2	70	10	20	92.9%	DW – 44.3°C, 5 EM PD – 46.8°C, 30 EM
1	Lightly Focused 25 mm ROC	2	70	10	24	90.3%	DW – 41.8°C, 0.4 EM PD – 46.2°C, 16 EM
2	Strongly Focused 32.5 mm ROC	2	75	10	18	86.3%	DW – 39.3°C, .02 EM PD – 44.1°C, 3.9 EM BD – 58.3°C, 6×10^4 EM BV – 45.7°C, 17.1 EM
2	Strongly Focused 32.5 mm ROC *Cooled bile duct	2	75	10	18	81.3%	DW – 39.6°C, .03 EM PD – 45.7°C, 6.7 EM BD – 44.4°C, 16.2 EM BV – 45.9°C, 18.9 EM
3	Planar	2	75	10	48	60.1%	DW – 44.1°C,11.8 EM PD – 43.2°C, 2.33 EM BV – 42.9°C, 1.95 EM
4	Planar	2	75	7	29	79.8%	SW – 44.4°C, 13.3 EM PD – 44.6°C, 4.0 EM BV – 43.0°C, 0.9 EM

Table IV

Parameters and outcomes for patient anatomy hyperthermia simulations.

Case	Transducer Configuration	Freq. (MHz)	Applied intensity (W/cm^2)	Max tumor temp. (°C)	Cooling water temp. (°C)	Volume, % tumor > 40/43°C
1	Tubular (80° sector)	1	2.8	45.0	25	4.1 cm^3, 95.0%/1.4 cm^3, 32.8%
2	Planar	1.5	1.5	45.0	20	3.7 cm^3, 86.5%/0.9 cm^3, 20.4%
3	Planar	1.5	1.7	45.0	25	7.6 cm^3, 20.4%/1.4 cm^3, 3.8%
4	Planar	1.5	1.6	45.0	25	11.6 cm^3, 66.6%/2.4 cm^3, 13.7%